Journal of Alloys and Compounds 509 (2011) 396–401

Contents lists available at ScienceDirect

Journal of Alloys and Compounds

journal homepage: www.elsevier.com/locate/jallcom

Synthesis, characterization, shape-preserved transformation, and optical properties of $La(OH)_3$, $La_2O_2CO_3$, and La_2O_3 nanorods

Qiuying Mu, Yude Wang*

Department of Materials Science and Engineering, Yunnan University, Kunming 650091, People's Republic of China

ARTICLE INFO

Article history:
Received 1 May 2010
Received in revised form 8 September 2010
Accepted 8 September 2010
Available online 17 September 2010

Keywords:
Nanorods
Surfactant
Shape-preserved transformation
Photoluminescence

ABSTRACT

A simple method to directly synthesize stable and crystalline pure phase $La(OH)_3$ nanorods, with a diameter of around 15 nm and lengths in the range of 120–200 nm, was developed using cationic surfactant (cetyltrimethylammonium bromide, CTAB). The obtained $La(OH)_3$ nanorods can be successfully converted to $La_2O_2CO_3$ and La_2O_3 nanorods via calcination under appropriate conditions. Analytical methods such as X-ray diffraction (XRD) spectra, Fourier transformed infrared (FTIR) spectrum, differential scanning calorimetry and thermogravimetric analysis (DSC–TGA), transmission electron microscopy (TEM), and high-resolution TEM (HRTEM) were employed to characterize the morphology and microstructure of the final products. The results reveal that $La(OH)_3$ nanorods were shape-preserved and transformed to $La_2O_2CO_3$ nanorods at 400 °C for 2 h and to La_2O_3 nanorods at 800 °C for 2 h, respectively. TEM images indicate that the as-obtained $La_2O_2CO_3$ and La_2O_3 entirely consist of uniform nanorods in high yield with diameters of about 15 nm and 23 nm, lengths of 200–300 nm and 300–500 nm, respectively. The formation mechanism of the $La(OH)_3$, $La_2O_2CO_3$ and La_2O_3 nanorods was investigated. Room-temperature photoluminescence (RTPL) properties were investigated under the excitation of 275 nm. The $^5D_3 \rightarrow {}^7F_j$ (j = 2–6) emission peaks at the wavelength below 500 nm were found in the RTPL spectra.

1. Introduction

Lanthanides are an attractive class of elements and have unique optical, catalytic, and magnetic properties because of their unique electron configuration (4f electrons). Lanthanum, the lightest element in the lanthanide series, has been widely studied in its oxide, hydroxide, oxycarbonate, phosphate, or oxychloride forms and has been extensively applied in optoelectronic devices [1–3], phosphors [4], solid electrolyte [5], catalytic [6–10], sorbent [11], and gas sensor [12]. Lanthanum hydroxide ($La(OH)_3$) is one of the novel rare earth compounds, and has been used in many fields, such as ceramic, superconductive materials, hydrogen storage materials, electrode materials, etc., especially catalyst and sorbent materials [13,14]. Lanthanum oxycarbonate ($La_2O_2CO_3$) is of considerable interest because of the impressive activity in various lanthanum-based catalysts [15–17]. Among various lanthanum-based materials, lanthanum oxide (La_2O_3) is particularly interesting material because it has several attractive properties for applications and is currently used as high k gate dielectric materials [18], optical filters [19], and catalysts [20,21]. Most of these advanced functions depend strongly on the compositions and structures, which are sensitive to the bonding states of rare earth atoms or ions. One-dimensional (1D) nanostructures, such as nanowires, nanobelts, nanotubes, and nanorods were prepared and used in a lot of fields. Owing to their unique physical and chemical properties, they were thus expected to be critical to the function and integration of nanoscale devices [22]. A one-dimensional (1D) nanostructured lanthanum oxide would hold promise as highly functionalized materials and act as electrically, magnetically, or optically functional host materials.

Various chemical methods are adopted for the preparation of lanthanum hydroxide nanostructures, including solvothermal [23], hydrothermal [24,25], hydrothermal microemulsion [26], and composite-hydroxide-mediated (CHM) [27]. The synthesis of these nanostructures was based on the preparation of rare earth hydroxide colloidal precipitates and the subsequent hydrothermal treatment at a designated temperature. The nanostructure morphologies were tuned by changing experimental parameters. In this paper, a facile method to prepare $La(OH)_3$ nanorods is described. Our method is based on the cationic surfactant CTAB and the simple chemical reagents (hydrous lanthanum chloride ($LaCl_3{\cdot}6H_2O$) and $NH_3{\cdot}H_2O$). The cations (lanthanum) are assembled within the template of surfactant micelle in an aqueous solution. Surfactant plays an important role in the preparation of $La(OH)_3$ nanorods. The surfactant not only provides favorable site for the growth of the particulate assemblies, it also influences the formation process, including nucleation, growth, coagulation, and flocculation [28]. $La_2O_2CO_3$ and La_2O_3 nanorods were produced from $La(OH)_3$

* Corresponding author.
E-mail address: ydwang@ynu.edu.cn (Y. Wang).

0925-8388/$ – see front matter © 2010 Elsevier B.V. All rights reserved.
doi:10.1016/j.jallcom.2010.09.041

precursors via heating treatment. This is the first synthesis of $La_2O_2CO_3$ with rod-like morphology, which may find important applications as gas sensors [29] and catalysts, owing to the 1D nanorods. A variety of different 1D morphologies of La_2O_3 crystals, including nanoneedles, nanorods, and nanorods bundles [30,31] has been prepared. Herein, we demonstrated a simple synthesis of La_2O_3 nanorods through $La(OH)_3$ precursor conversion. La_2O_3 nanorods with diameters of approximately 23 nm and lengths of 300–500 nm have been successfully obtained. The structure and morphology of the maintained products were studied by X-ray diffraction (XRD), Fourier transformed infrared (FTIR) spectra, differential scanning calorimetry and thermogravimetric analysis (DSC–TGA), high-resolution transmission electron microscopy (HRTEM), and RTPL spectra.

2. Experimental

2.1. Synthesis of materials

All chemical reagents used in the experiments were obtained from commercial sources as guaranteed-grade reagents and used without further purification. The purity of CTAB was 99% and the purities of the inorganic precursors were not less than 99.90% respectively.

The synthesis of lanthanum hydroxide ($La(OH)_3$) nanorods was based on the cationic surfactant (CTAB) and the simple chemical materials (lanthanum chloride hexahydrate $LnCl_3{\cdot}6H_2O$ and $NH_3{\cdot}H_2O$) as inorganic precursors. The synthesis procedures were carried out at room temperature. In a typical process, the synthesis procedure was as follows: The CTAB (6 mmol) was dissolved in 20 ml distilled water with slowly stirring for several minutes until a clear homogeneous solution was obtained. The $LaCl_3{\cdot}6H_2O$ (4 mmol) was mixed with distilled water (10 ml) until a homogenous solution was obtained. The solution of $LaCl_3$ was then added into the obtained CTAB solution with stirring. After stirring 30 min, the mixing solution became homogeneous, a solution of diluted $NH_3{\cdot}H_2O$ (25–28 wt% solution, 48 ml) was added into with vigorous stirring. A white precipitate of $La(OH)_3$ appeared immediately. Then the above mixing solution was stirred for 2 h at room temperature. The products were aged at ambient temperature at 55 days. The final products were collected by filtering, washing with distilled water to remove surfactant and then dried in an oven at 60 °C.

Lanthanum oxide carbonate ($La_2O_2CO_3$) nanorods were obtained by annealing the lanthanum hydroxide ($La(OH)_3$) nanorods in furnace at 400 °C for 2 h. The pure La_2O_3 nanorods could be successfully obtained by calcining the $La(OH)_3$ nanorods at 800 °C for 2 h.

2.2. Characterization of materials

The differential scanning calorimetry and thermogravimetric analysis (DSC–TGA) curves were obtained in flowing air on NETZSCH STA 409 PG/PC with a temperature increasing rate of 10 °C/min. X-ray diffraction (XRD, Rigaku D/MAX-3B powder diffractometer) with copper target and K_α radiation ($\lambda = 1.54056$ Å) was used for the phase identification, where the diffracted X-ray intensities were recorded as a function of 2θ. The sample was scanned from 10° to 80° (2θ) in steps of 0.02°. Fourier transform infrared (FTIR) investigations were performed on a Perkin-Elmer 2000 FTIR spectrometer. Transmission electron microscopy (TEM) measurement was performed on a Zeiss EM 912 Ω instrument at an acceleration voltage of 120 kV, while high-resolution transmission electron microscopy (HRTEM) characterization was done using JEOL JEM-2010 Electron Microscope (with an acceleration voltage of 200 kV). The samples for TEM were prepared by dispersing the final samples in distilled water, and this dispersing was then dropped on carbon–copper grids covered by an amorphous carbon film. To prevent agglomeration of nanorods the copper grid was placed on a filter paper at the bottom of a Petri dish. Room-temperature photoluminescence (RTPL) experiments were measured on a Hitachi F-4500 FL Spectrophotometer using a Xenon lamp as the excitation source at room temperature. All experiments were performed at room temperature.

3. Results and discussion

Lanthanum hydroxides may become carbonate when exposed to the air (Eq. (1)) and the presence of CO_3^{2-} and/or HCO_3^- was checked [32]. The TGA and DSC measurements were carried out in a flowing air atmosphere to analyze the decomposition process of the as-prepared $La(OH)_3$ nanorods. A representative DSC–TGA profile under a flowing air is shown in Fig. 1. It can be seen that the reactions are divided into three temperature regions. The first is over the temperature range from room temperature to ca. 150 °C,

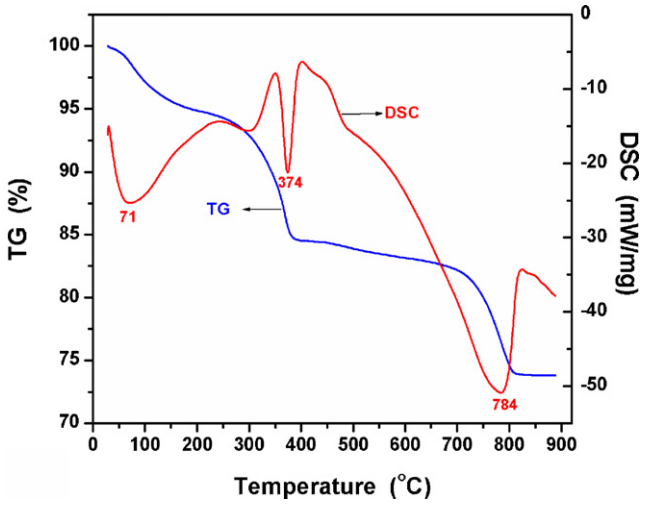

Fig. 1. DSC and TGA curves of as-synthesized $La(OH)_3$ sample.

the second is over the temperature range from 150 °C to 400 °C, the third is at 400–800 °C. Presumably, the first effect is attributed to the release of the adsorbed water on the $La(OH)_3$ nanorods surface and the forming lanthanum carbonate $La_2O(CO_3)_2{\cdot}xH_2O$ (Eq. (2)). This process corresponds to about 5% total weight loss. In the range of 150–400 °C, it gives off the remaining water (Eq. (3)) and lanthanum oxide carbonate is decomposed to $La_2O_2CO_3$ and corresponds to about 11.6% weight loss (Eq. (4)). In the range of 400–800 °C, $La(OH)_3$ and $La_2O_2CO_3$ are gradually decomposed into La_2O_3 (Eq. (5)). The theoretical mass losses of $La(OH)_3$ to $La_2O_2CO_3$ and $La_2O_2CO_3$ to La_2O_3 are 12.7 and 11.9 mass%, respectively. The experimental values are 16.0 mass% between room-temperature and 400 °C and 10.7 mass% from 400 °C to 800 °C. The actual weight loss is more than that calculated from these reaction processes, which indicated that some organic residua CTAB may exist in the initial $La(OH)_3$ product and were burned off during this temperature range. Based on these results, a pathway for the decomposition of $La(OH)_3$ is proposed as follows:

$$La(OH)_3 + CO_2 \rightarrow LaOHCO_3 \quad (1)$$

$$LaOHCO_3 \rightarrow La_2O(CO_3)_2{\cdot}xH_2O + yH_2O \quad (2)$$

$$La_2O(CO_3)_2{\cdot}xH_2O \rightarrow La_2O(CO_3)_2 + xH_2O \quad (3)$$

$$La_2O(CO_3)_2 \rightarrow La_2O_2CO_3 + CO_2 \quad (4)$$

$$La_2O_2CO_3 \rightarrow La_2O_3 + CO_2 \quad (5)$$

Little further weight loss in the TGA curve was observed at a temperature above 800 °C, indicating the completion of any reaction involving a weight change. Due to the much lower heating rate in the synthesis (TGA measurements were performed with 10 °C/min, in contrast to only 5 °C/min heating in the calcination program which in addition contained 2 h holding steps at 800 °C), it is therefore safe to say that $La(OH)_3$ and $La_2O_2CO_3$ are finally decomposed into La_2O_3 in the calcination step.

Fourier transform infrared (FTIR) spectroscopy was usually employed as an additional probe to evidence the presence of OH groups as well as other organic and inorganic species. The FTIR spectra in the range 4000–400 cm^{-1} of the products are shown in Fig. 2. For the $La(OH)_3$ nanorods, the inexistence of CH_2 vibrations at 2846.4 cm^{-1} and 2918.7 cm^{-1} indicates that the surfactant is not present in the as-synthesized sample. An intense and sharp band at 3609.4 cm^{-1} is assigned to the stretching and bending O–H vibrations of lanthanum hydroxide [33–37]. The bands at 3421.4 cm^{-1} and 1631.3 cm^{-1} can be attributed to the O–H vibration in absorbed water on the sample surface [38]. The sharp peak at 1333.9 cm^{-1} is

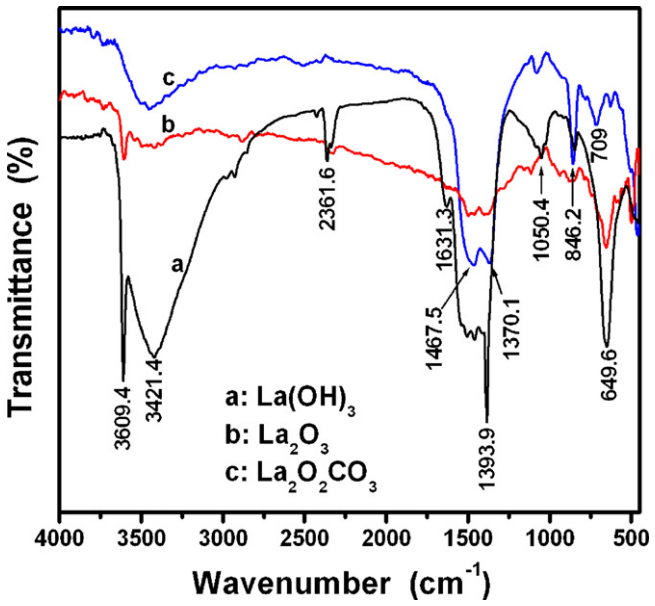

Fig. 2. FTIR spectra of $La(OH)_3$ (a), La_2O_3 (b), and $La_2O_2CO_3$ (c) nanorods.

due to the bending mode of O–H. The bands at around 649.6 cm^{-1} assigned to the bend vibration of La–O–H [33–37]. The peaks of the FTIR bands at 846, 1050, 2361 or 1478 cm^{-1} are assigned to CH_2, C–O, C≡N stretching vibration, and CH_3 antisymmetric stretching vibration, respectively. We attribute this to the $La(OH)_3$ surface with a little of the rudimental CTAB and the carbonate reacting with CO_2 in air.

The phase purity of the products was examined by X-ray diffraction (XRD) measurement performed on Rigaku X-ray diffractometer with Cu Kα radiation. All diffraction peaks in Fig. 3a can be perfectly indexed to a pure hexagonal phase [space group: $P6_3/m$ (176)] of $La(OH)_3$ with lattice constants $a = 6.528$ Å, $c = 3.858$ Å (JCPDS No. 36-1481). Fig. 3b shows that pure-phase $La_2O_2CO_3$ can be obtained by calcination of as-made $La(OH)_3$ at 400 °C for 2 h. All diffraction peaks of XRD pattern can be indexed to a pure phase of $La_2O_2CO_3$ with lattice constants $a = 4.080$ Å, $b = 13.50$ Å, $c = 4.072$ Å (JCPDS No. 48-1113). With increasing of calcination temperature,

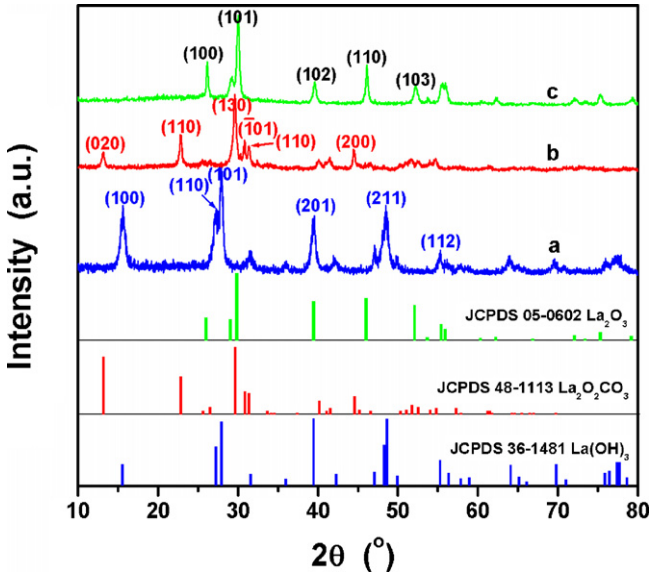

Fig. 3. X-ray diffraction analysis of $La(OH)_3$ (a), $La_2O_2CO_3$ (b), and La_2O_3 (c) nanorods.

$La(OH)_3$ and $La_2O_2CO_3$ are gradually decomposed into La_2O_3. After calcination at 800 °C for 2 h, a pure phase of La_2O_3 with lattice constants $a = 3.973$ Å, $c = 6.129$ Å (JCPDS No. 05-0602) is observed in Fig. 3c. No other impurity peaks are detected, indicating that the $La(OH)_3$ and $La_2O_2CO_3$ have been converted into the hexagonal La_2O_3 phase completely during the calcination conversion process. Table 1 lists the data of the phase structures and the lattice constants of $La(OH)_3$, $La_2O_2CO_3$, and La_2O_3.

The morphologies of the as-obtained $La(OH)_3$, $La_2O_2CO_3$, and La_2O_3 samples were investigated by TEM images. Fig. 4a shows the typical image of $La(OH)_3$ nanorods. TEM observation revealed that they all exhibited one-dimensional rod-like nanostructures of hexagonal structure. The $La(OH)_3$ nanostructures synthesized by the process display the uniform morphology of nanorods with 13–15 nm in width and 150–200 nm in length. That is to say, the aspect ratios of these rods are about 10–15. The HRTEM image of $La(OH)_3$ nanorods shown in Fig. 4b indicates that the nanorod is structurally uniform with an interplanar spacing of about 0.32 nm, which corresponds to the (1 0 1) plane of hexagonal $La(OH)_3$.

The simple chemical reaction for the precipitation of $La(OH)_3$ is proposed as follows:

$$La^{3+} + 3OH^- \rightarrow La(OH)_3 \quad (6)$$

Template-based systems are frequently used to control nucleation and growth of inorganic particles. In this approach, the template simply serves as a scaffold with (or around) which a different material is generated in situ and shaped into a nanostructure with its morphology complementary to that of the template. When the solutions (CTAB and $LaCl_3 \cdot 6H_2O$ mixed solution and $NH_3 \cdot H_2O$ solution) were mixed, the white precipitate appeared at once and gradually increased with the adding of $NH_3 \cdot H_2O$ solution, which indicated that the reaction happened. On the basis of the series of experimental data, the overall assembly behaviors of the $La(OH)_3$ nanorods at room temperature could be illustrated as in Fig. 5a and b. The similar formation mechanisms were reported and the generating 1D nanostructures in relatively large quantities can be synthesized by templating against rod-like micelles assembled from CTAB [39–43]. In this case, the formation of the $La(OH)_3$ nanorods belongs to a self-assembly process. After calcination under appropriate conditions, $La(OH)_3$ nanorods were shape-preserved and transformed to $La_2O_2CO_3$ nanorods and to La_2O_3 nanorods, respectively.

In recent years, the research of new rare-earth luminescent materials has received great attention, since new luminescent materials may have the capacity to solve existing problems. In order to improve the material properties, it is generally required to use nanostructures with controlled shape and size as starting materials. Designing systems with lower dimensionality like nanofibers, nanowires, nanobelts or nanorods is of great importance due to the

Table 1
The phase structures and lattice constants of $La(OH)_3$, $La_2O_2CO_3$, and La_2O_3 nanorods.

	ICDD PDF no.	JCPDS			Average lattice constant		
		a (Å)	b (Å)	c (Å)	a (Å)	b (Å)	c (Å)
$La(OH)_3$	36–1481	6.528	6.528	3.858	6.556	6.556	3.839
$La_2O_2CO_3$	48–1113	4.080	13.50	4.072	4.078	13.42	4.026
La_2O_3	05–0602	3.973	3.973	6.129	3.941	3.941	6.092

$La(OH)_3$: the average lattice constant was calculated from (1 0 0), (1 1 0), (1 0 1), (2 0 1), (2 1 1) and (1 1 2) reflections. JCPDS 36-1481, system: hexagonal, lattice: primitive, space group: $P6_3/m$(176). $La_2O_2CO_3$: the average lattice constant was calculated from (0 2 0), (1 1 0), (1 3 0), ($\bar{1}$ 0 1), (1 0 1) and (2 0 0) reflections. JCPDS 48-1113, system: monoclinic, lattice: primitive, space group: $P6_3/mmc$. La_2O_3: the average lattice constant was calculated from (1 0 0), (1 0 1), (1 0 2), (1 1 0) and (1 0 3) reflections. JCPDS 05-0602, system: hexagonal, lattice: primitive, space group: $P\bar{3}m1$(164).

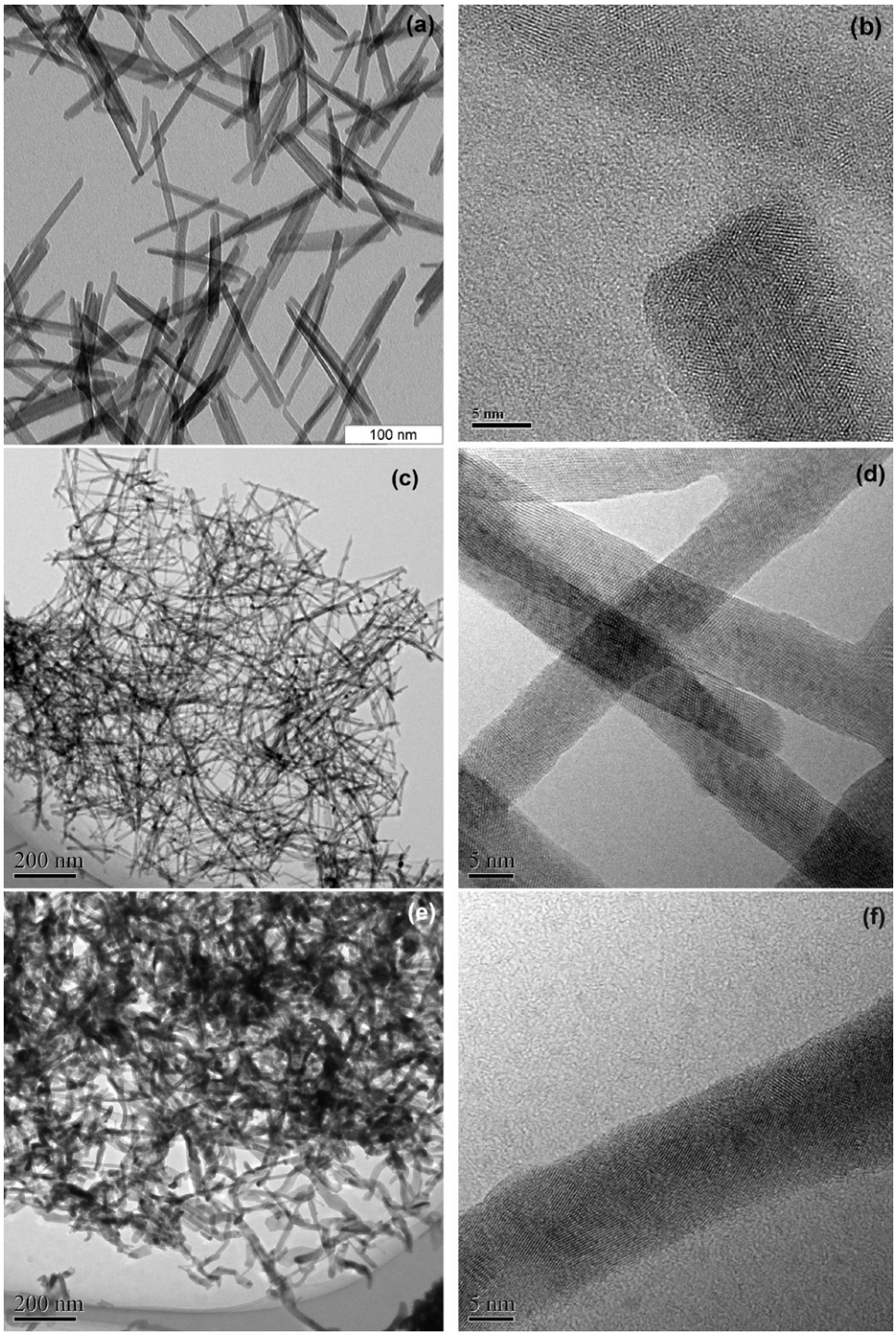

Fig. 4. TEM and HRTEM images of $La(OH)_3$, La_2O_3, and $La_2O_2CO_3$ nanorods.

possible novel properties induced by the reduced dimensionality [44,45]. UV/vis spectroscopy was used to characterize the optical absorbance of the $La(OH)_3$, $La_2O_2CO_3$, and La_2O_3 nanorods. The absorption spectra of these nanorods were carried out to resolve the excitonic or interband (valence–conduction band) transition, which allows us to calculate the band gap. The UV/vis absorption spectra of $La(OH)_3$, $La_2O_2CO_3$, and La_2O_3 nanorods show the strong band edge absorption in the region under 250 nm (Fig. 6). It is well known that the absorption coefficient of an amorphous semiconductor has a characteristic relation [46]:

$$(\alpha h\nu)^{1/2} = B(h\nu - E_g) \quad (7)$$

in which $h\nu$ is the photon energy, E_g is the apparent optical band gap, B is a constant characteristic of the semiconductor, and α is the absorption coefficient. Therefore, the E_g of the resulted $La(OH)_3$, $La_2O_2CO_3$, and La_2O_3 nanorods can be obtained by the extrapolation of the above relation to be 4.35–5.38 eV (see Fig. 6, inset). The E_g values of $La_2O_2CO_3$ and La_2O_3 nanorods are 5.04 eV and 4.35 eV, respectively, which are higher than the E_g values of $La_2O_2CO_3$ and La_2O_3 calculated based on first-principles pseudopotential calculation as 3.65 eV and 3.8 eV [27]. We think that the nanostructure plays a major role in E_g value increase. This is similar to the quantum size effect, which leads to a blue-shift of E_g with decreasing particle size, and has

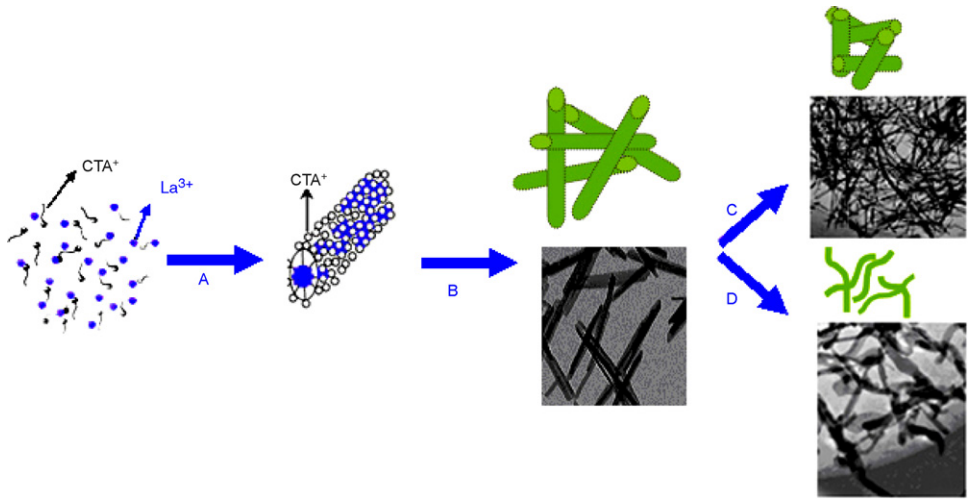

Fig. 5. Schematic diagram of the proposed mechanism for the formation of the $La(OH)_3$, $La_2O_2CO_3$, and La_2O_3 nanorods in room temperature. (a) Surfactant–inorganic ions interaction, (b) inorganic ions polymerization and inorganic ions–hydroxyl interaction to form $La(OH)_3$ nanorods, (c) $La(OH)_3$ nanorods were calcined at 400 °C to form $La_2O_2CO_3$ nanorods, and (d) $La(OH)_3$ nanorods were calcined at 800 °C to form La_2O_3 nanorods.

been observed in many nanometer-sized semiconductor materials [47].

To explore the possibilities of luminescent properties by $La(OH)_3$, $La_2O_2CO_3$, and La_2O_3 nanorods, we carried out PL measurements at room temperature. The room temperature emission spectrum of these nanorods is shown in Fig. 7. In our investigation, room temperature photoluminescence spectra were performed with an excitation wavelength (λ_{ex} = 275 nm). As shown in Fig. 7, the main emission peaks at the wavelength below 500 nm were found in the PL spectra. There are five strong peaks at 452.1 nm, 463.9 nm, 468.8 nm, 482.6 nm, and 493.4 nm at the room temperature. The strongest emission band was located at 468.8 nm, which is a typical blue band. They are attributed, respectively, to the $^5D_3 \rightarrow {}^7F_j$ (j = 2–6). The photoluminescence properties of the $La(OH)_3$, $La_2O_2CO_3$, and La_2O_3 nanorods are not varied and dependent upon the different lanthanum compounds. La^{3+} has not any luminescence because of the zero electrons in the 4f shell, and La cannot be regarded as an emission center and cannot radiate light

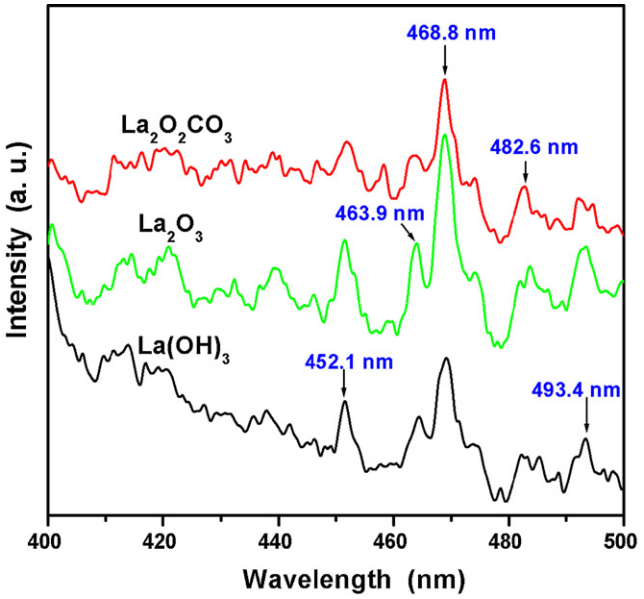

Fig. 7. Room-temperature photoluminescence spectra of $La(OH)_3$, $La_2O_2CO_3$, and La_2O_3 nanorods.

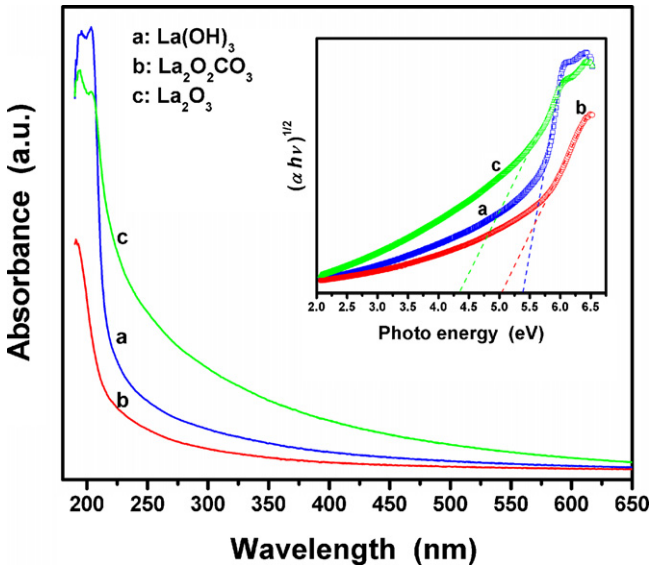

Fig. 6. Absorption spectra of $La(OH)_3$, $La_2O_2CO_3$, and La_2O_3 nanorods. Inset: apparent energy gap of $La(OH)_3$, $La_2O_2CO_3$, and La_2O_3 nanorods from the extrapolation of Urbach's equation.

from the inner atomic 4f shell [27,48]. The emission of 468.8 nm could not contribute to the transition from the conduction band to the valence band. The emission does not originate from a transition between the conduction and valence band, while comes from a deep-level or trap-state emission. The morphology of the nanorods suggests that they play a major role in the emission origination. The similar results can be found in reference reported by Wang and colleagues [27]. Further work is to be done to get a definite understanding.

4. Conclusions

In this study, stable and crystalline pure phase $La(OH)_3$ nanorods of hexagonal structure with a diameter of around 15 nm and lengths in the range of 120–200 nm were successfully synthesized by a facile process at room temperature. $La(OH)_3$ nanorods were shape-preserved and transformed to $La_2O_2CO_3$ nanorods by calcination at 400 °C for 2 h and to La_2O_3 nanorods at 800 °C for 2 h,

respectively. According to the XRD and HRTEM patterns, the as-obtained $La_2O_2CO_3$ and La_2O_3 entirely consist of uniform nanorods with diameters of about 15 nm and 23 nm, lengths of 200–300 nm and 300–500 nm, respectively. It is considered that this simple method can be applied as a general method for the preparation of rare-earth hydroxides with 1D nanostructures. RTPL properties were investigated under the excitation of 275 nm and the samples exhibited the emission peaks of room-temperature photoluminescence, which are attributed to the $^5D_3 \rightarrow {}^7F_j$ (j = 2–6), respectively.

Acknowledgement

This work was supported by the Graduate Research Project of Yunnan University, China (No. ynuy200935).

References

[1] A.A. Dakhel, Colloids Surf. A: Physicochem. Eng. Aspect 332 (2009) 9–12.
[2] P. Schuetz, F. Caruso, Chem. Mater. 14 (2002) 4509–4516.
[3] H. Meyssamy, K. Riwotzki, A. Kornowski, S. Naused, M. Haase, Adv. Mater. 11 (1999) 840–844.
[4] M. Ferhi, K. Horchani-Naifer, M. Férid, J. Lumin. 128 (2008) 1777–1782.
[5] N. Imanaka, K. Okamoto, G.Y. Adachi, Angew. Chem. Int. Ed. 41 (2002) 3890–3892.
[6] A. Slagtern, Y. Schuurman, C. Leclercq, X. Verykios, C. Mirodatos, J. Catal. 172 (1997) 118–126.
[7] E. Ordonez-Regil, R. Drot, E. Simoni, J.J. Ehrhardt, Langmuir 18 (2002) 7977–7984.
[8] S.J. Huang, A.B. Walters, M.A. Vannice, J. Catal. 192 (2000) 29–47.
[9] C.H. Lin, K.D. Campbell, J.X. Wang, J.H. Lunsford, J. Phys. Chem. 90 (1986) 534–537.
[10] P. Chanaud, A. Julbe, P. Vaija, M. Persin, L. Cot, J. Mater. Sci. 29 (1994) 4244–4251.
[11] S. Tokunaga, S.A. Wasay, S.W. Park, Water Sci. Technol. 35 (1997) 71–78.
[12] N. Imanaka, K. Okamoto, N.G. Adachi, Electrochem. Commun. 3 (2001) 49–51.
[13] J.L. Zhu, Y.H. Zhou, H.X. Yang, J. Power Sources 69 (1997) 169–173.
[14] M.P. Rosynek, D.T. Magnuson, J. Catal. 46 (1977) 402–413.
[15] R. Taylor, G. Schrader, Ind. Eng. Chem. Res. 30 (1991) 1016–1023.
[16] A.N. Fatsikostas, D.I. Kondarides, X.E. Verykios, Catal. Today 75 (2002) 145–155.
[17] F. Frusteri, S. Freni, V. Chiodo, L. Spadaro, O.D. Blasi, G. Bonura, S. Cavallaro, Appl. Catal. A 270 (2004) 1–7.
[18] S.W. Kang, S.W. Rhee, J. Electrochem. Soc. 149 (2002) C345–C348.
[19] S. Wang, W. Wang, Y. Qian, Thin Solid Films 372 (2000) 50–53.
[20] B.S. Sanchez, C.A. Querini, E.E. Miro, Appl. Catal. A 366 (2009) 166–175.
[21] L. Tang, Y. Li, K.L. Xu, X.D. Hou, Y. Lv, Sen. Actuators B 132 (2008) 243–249.
[22] J.T. Hu, T.W. Odom, C.M. Lieber, Acc. Chem. Res. 32 (1999) 435–445.
[23] B. Tang, J.C. Ge, C.J. Wu, Nanotechnology 15 (2004) 1273–1276.
[24] X.Y. Ma, H. Zhang, Y.J. Ji, J. Xu, D. Yang, Mater. Lett. 58 (2004) 1180–1182.
[25] X. Wang, Y.D. Li, Angew. Chem. Int. Ed. 41 (2002) 4790–4793.
[26] Y.D. Yin, G.Y. Hong, Chin. Chem. Lett. 16 (2005) 1659–1662.
[27] C.G. Hu, H. Liu, W. Dong, Y.Y. Zhang, G. Bao, C.S. Lao, Z.L. Wang, Adv. Mater. 19 (2007) 470–474.
[28] S.G. Dixit, A.R. Mahadeshwar, S.K. Haram, Colloids Surf. A: Physicochem. Eng. Aspect 133 (1998) 69–75.
[29] I. Djerdj, A. Haensch, D. Koziej, S. Pokhrel, N. Barsan, U. Weimar, M. Niederberger, Chem. Mater. 21 (2009) 5375–5381.
[30] J. Sheng, S. Zhang, S. Lv, W.D. Sun, J. Mater. Sci. 42 (2007) 9565–9571.
[31] N. Zhang, R. Yi, L.B. Zhou, G.H. Gao, R.R. Shi, G.Z. Qiu, X.H. Liu, Mater. Chem. Phys. 114 (2009) 160–167.
[32] Q.Y. Mu, T. Chen, Y.D. Wang, Nanotechnology 20 (2009) 345602 (7pp).
[33] H.B. Zhang, H.S. Liu, X.J. Cao, S.J. Li, C.C. Sun, Mater. Chem. Phys. 79 (2003) 37–42.
[34] H.L. Zhu, D.R. Yang, H. Yang, L.M. Zhu, D.S. Li, D.L. Jin, K.H. Yao, J. Nanopart. Res. 10 (2008) 307–312.
[35] T. Levan, M. Che, J.M. Tatibouet, M. Kermarec, J. Catal. 142 (1993) 18–26.
[36] S. Bernal, F.J. Botana, R. García, J.M. Rodríguez-Izquierdo, React. Solids 4 (1987) 23–40.
[37] G. Busca, V. Lorenzelli, Mater. Chem. 7 (1982) 89–126.
[38] G. Zou, R. Liu, W. Chen, Z. Xu, Mater. Res. Bull. 42 (2007) 1153–1158.
[39] Y.N. Xia, P.D. Yang, Y.G. Sun, Y.Y. Wu, B. Mayers, B. Gates, Y.D. Yin, F. Kim, H.Q. Yan, Adv. Mater. 15 (2003) 353–389.
[40] M. Li, H. Schnablegger, S. Mann, Nature 402 (1999) 393–395.
[41] S. Kwan, F. Kim, J. Akana, P.D. Yang, Chem. Commun. (2001) 447–448.
[42] Y.Y. Yu, S.S. Chang, C.L. Lee, C.R.C. Wang, J. Phys. Chem. B 101 (1997) 6661–6664.
[43] M.A. El-Sayed, Acc. Chem. Res. 34 (2001) 257–264.
[44] I. Djerdj, G. Garnweitner, D.S. Su, M. Niederberger, J. Solid State Chem. 180 (2007) 2154–2165.
[45] I. Djerdj, D. Arčon, Z. Jagličić, M. Niederberger, J. Solid State Chem. 181 (2008) 1571–1581.
[46] G. Mill, Z.G. Li, D. Meisel, J. Phys. Chem. 92 (1988) 822–828.
[47] X.C. Wu, B.S. Zou, J.R. Xu, B.L. Yu, G.Q. Tang, G.L. Zhang, W.J. Chen, Nanostruct. Mater. 8 (1997) 179–189.
[48] J.Y. Li, Luminescent Materials of Rare Earths and their Applications, Chemical Industry Press, Beijing, 2003.